scientific reports

Check for updates

OPEN

The impact of pericytes on the stability of microvascular networks in response to nanoparticles

Matthew Dibble[1,2], Stefania Di Cio'[1,2], Piaopiao Luo[1,2], Frances Balkwill[1,3] & Julien E. Gautrot[1,2]✉

Recapitulating the normal physiology of the microvasculature is pivotal in the development of more complex in-vitro models and organ-on-chip designs. Pericytes are an important component of the vasculature, promoting vessel stability, inhibiting vascular permeability and maintaining the vascular hierarchical architecture. The use of such co-culture for the testing of therapeutics and nanoparticle safety is increasingly considered for the validation of therapeutic strategies. This report presents the use of a microfluidic model for such applications. Interactions between endothelial cells and pericytes are first explored. We identify basal conditions required to form stable and reproducible endothelial networks. We then investigate interactions between endothelial cells and pericytes via direct co-culture. In our system, pericytes prevented vessel hyperplasia and maintained vessel length in prolonged culture (> 10 days). In addition, these vessels displayed barrier function and expression of junction markers associated with vessel maturation, including VE-cadherin, β-catenin and ZO-1. Furthermore, pericytes maintained vessel integrity following stress (nutrient starvation) and prevented vessel regression, in contrast to the striking dissociation of networks in endothelial monocultures. This response was also observed when endothelial/pericyte co-cultures were exposed to high concentrations of moderately toxic cationic nanoparticles used for gene delivery. This study highlights the importance of pericytes in protecting vascular networks from stress and external agents and their importance to the design of advanced in-vitro models, including for the testing of nanotoxicity, to better recapitulate physiological response and avoid false positives.

The vasculature is an integral component of many physiological and pathophysiological conditions and its formation and stabilisation in-vitro are essential for the development of vascularised tissue models[1–5]. Such 3D *in-vitro* models are important for the accurate prediction of drug and nanomaterial toxicity, particularly considering the ubiquity of particle exposure (metallic, ceramic and polymeric) in daily life[6,7]. Traditional 2D systems lack physiological characteristics (geometry, mechanical and biochemical stimuli) which might lead to misrepresentation of normal physiological in-vivo processes and their response to fine chemicals, therapeutic agents and nanomaterials. Although 2D models have been useful in identifying the potential impact of such compounds on endothelial biology and barrier function of the endothelium[8], and remain more adapted to high throughput screening, 3D models emerge as useful alternatives for more accurate prediction of safety and efficacy testing[2,9]. The emergence of organ-on-a-chip systems is crucial in this effort and allows, for example, the addition of flow and biochemical gradients[10]. Atmospheric nanoparticles were found to increase vessel permeability by disrupting barrier functions in a 3D vasculature-on-a-chip model[11]. Using another 3D microvessel-on-a-chip system, the extravascular transport mechanism of cationic polymer nanoparticles was assessed[12].

Researchers have developed various iterations of a 'vasculature-on-a-chip'[3,13–20]. These models generally use PDMS chips which are manufactured using photo- and soft-lithography. A relatively established design features a central gel compartment flanked by lateral medium compartments, separated by microposts. The central gel compartment is injected with a hydrogel precursor, together with endothelial cells, followed by culture to allow

[1]School of Engineering and Materials Science, Institute of Bioengineering, Queen Mary, University of London, Mile End Road, London E1 4NS, UK. [2]School of Engineering and Materials Science, Queen Mary, University of London, Mile End Road, London E1 4NS, UK. [3]Barts Cancer Institute, Queen Mary, University of London, Charterhouse Square, London EC1M 6BQ, UK. ✉email: j.gautrot@qmul.ac.uk

the assembly of a microvasculature and the maturation of its lumenised structure. Microfluidic devices offer several advantages over more traditional in-vitro blood vessel models, including co-culture potential, real-time imaging, and physiological architecture. However, some of the parameters regulating the formation of such microvasculature on chips (concentrations of fibrinogen, thrombin, aprotinin, endothelial cell density, presence of stromal cells and exogenous factors) have not been studied systematically to rigorously compare and present their impact on network maturation[13,16,20–24]. Such variation in conditions can lead to poor reproducibility and makes direct comparison between different studies limited. A side-by-side comparison of the importance of these different factors is therefore important for the wider implementation of these models by the bioengineering community.

One common problem encountered when culturing microvasculatures for prolonged times (> 4 days) is vessel hyperplasia. This could limit long-term culture and the use of these systems for embedding spheroids and organoids for the development of advanced tissue models. To overcome this issue, endothelial cells can be cultured with pericytes[15–17]. Pericytes are abluminally located mesenchymal cells that have the capacity to differentiate in many types of cells[25]. Due to their heterogeneity, the identification of specific markers has been disputed[26], but platelet-derived growth factor receptor-β (PDGFRβ) and neural/glial antigen-2 (NG2) are generally accepted markers associated with these cells[27,28]. Pericytes typically interact with a number of endothelial cells, with primary cytoplasmic processes running along the abluminal surface of the endothelium and secondary processes running perpendicularly, enclosing the endothelial tube[29]. Co-culturing endothelial cells with pericytes inhibits vessel hyperplasia and endothelial cell proliferation and promotes vessel barrier function and endothelial cell survival[15,17,30–32].

In this study, we first examine the role of a range of parameters regulating the establishment of a stable microvasculature, including the effect of cell density, fibrinogen, collagen I, vascular endothelial growth factor (VEGF) and aprotinin concentrations. In addition, we study how pericytes stabilise endothelial network formation and impact on its barrier function. We then apply this system to the study of toxicity to the microvasculature, in the context of nanoparticle response.

Materials and methods

Microfabrication and material characterisation. *Microfluidic chip fabrication.* Microfluidic devices were fabricated using photo- and soft lithography. A master with positive relief patterns of SU-8 2050 photoresist (A-Gas Electronic Materials) on a silicon wafer (PI-KEM) was prepared by photolithography. A PDMS (Ellsworth Adhesives) polymer was cast against this master and thermally cured to obtain a negative replica piece. After separating from the master, hydrogel ports and medium reservoirs were punched from the PDMS stamp using biopsy punches. The PDMS stamp is then bonded to a glass coverslip using an oxygen plasma treatment. Devices were then autoclaved and dried at > 60 °C for 3 days to restore hydrophobicity.

Contact angle goniometry. Contact angle goniometry was used to investigate PDMS hydrophobic recovery post-plasma treatment. Samples were exposed to a 5 µL deionised water droplet and the contact angle between the PDMS and water droplet was extrapolated using the 'Default Method' of the DSA 100 (Kruss Scientific, Advance v2) software. Three replicates per repeat were quantified.

Cell culture. *General cell culture protocols.* Human umbilical vein endothelial cells (HUVECs) were obtained from Lonza and cultured in Endothelial Growth Medium-2 (EGM-2, Lonza) or EGM-2 BulletKit (Lonza), with passages 2–6 used in experiments. Human pericytes derived from placenta were obtained from Promocell and cultured in Pericyte Growth Medium (PGM, Promocell), with passages 2–6 used in experiments. HUVECs were detached using Versene/Trypsin (9:1), while Pericytes were detached using the Detach-30 kit (Promocell).

Vasculogenesis cell seeding. Cells were mixed in a fibrinogen solution and injected in the device gel channel via inlets (see Fig. 1A). Bovine fibrinogen (Sigma-Aldrich) and thrombin (Sigma-Aldrich) were separately dissolved in EGM-2 and DPBS, and mixed 1:1 to obtain final concentrations of 10 mg/mL and 2 U/mL, respectively. HUVECs or HUVECs/pericytes were pre-mixed in the thrombin solution to have a final cell density of 6×10^6 HUVECs/mL, or 6×10^6 HUVECs/mL + 6×10^5 pericytes/mL. After injection, devices are incubated for 5 min at 37 °C. The side-channels and media reservoirs are then filled with a total of 400 µL EGM-2 supplemented with VEGF (50 ng/mL, Peprotech). Culture Medium is replaced every 24 h.

Flow cytometry. We performed flow cytometry to confirm typical markers expressed by pericytes. Single cell suspensions of pericytes were stained for 30 min at room temperature (RT) using fluorescence-labelled antibodies for pericyte surface markers (488-NG2 from Invitrogen, APC PDGFR-β and APC CD105 from Biolegend) and DAPI for cell viability. Labelled cells were then washed in PBS + 1% BSA and were analyzed on a FACSCanto II flow cytometer (Becton Dickinson). Data analysis was performed using FlowJo software (Tree Star, v10).

FITC-dextran permeability assay. To investigate the impact of pericytes on vascular permeability and endothelial barrier function, an assay was established based on previous reports[15,23]. The vascular network was cultured according to the previously described protocol. Following 10-days culture, the medium reservoirs were aspirated and 30 µL EGM-2 containing 25 µg/mL 70 kDa FITC-dextran dye (Thermo Fisher Scientific) added to a single reservoir. FITC-dextran perfused through the vascular network allowing the visualisation and qualitative analysis of barrier function by recording dye diffusion across the endothelium into the extravascular com-

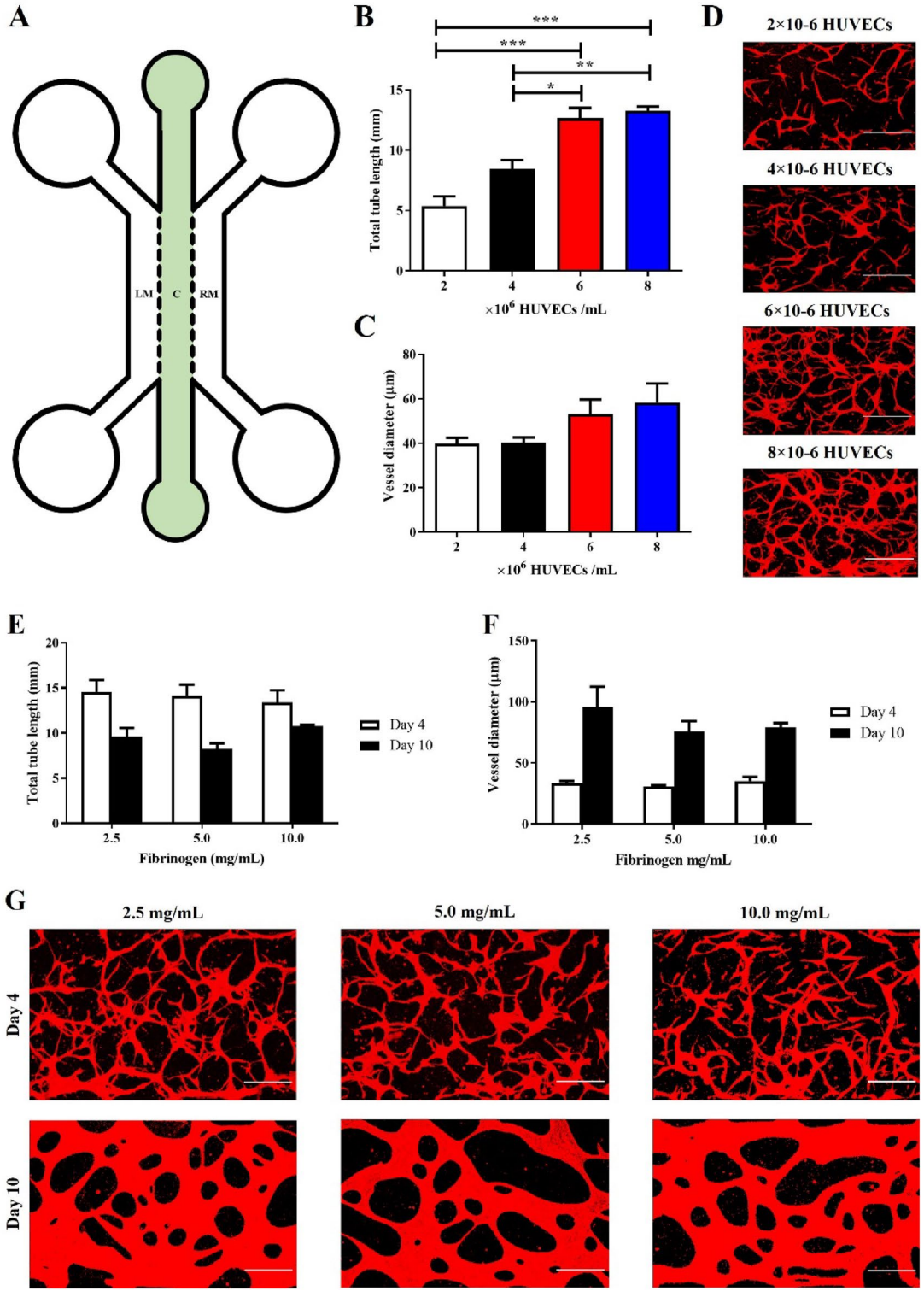

Figure 1. The impact of cell density and fibrinogen concentration on vasculogenesis. (**A**) Schematic of chip design. Central channel (noted c) is 1000 μm wide and separated from the lateral medium channels (LM and RM) by 300 μm long hexagonal posts, spaced by 75 μm gaps. (**B**) Increasing HUVEC density significantly increases total tube length (5.4 ± 0.8, 8.4 ± 0.7, 12.7 ± 0.9 and 13.3 ± 0.4 mm/field of view for 2, 4, 6, 8×10^6 HUVECs/mL respectively). (**C**) HUVEC density had no significant impact on vessel diameter (mean range 39.8–58.4 μm). (**D**) Representative images of different HUVEC densities, z-projection images were generated from confocal images. Red, F-actin. Scale bar: 300 μm. (**E**) Fibrinogen concentration had no significant impact on total tube length at day 4 (mean range 13.4–14.5 mm/field of view), or day 10 (mean range 8.2–10.7 mm/field of view). (**F**) Fibrinogen concentration also had no impact on vessel diameter following 4 days (mean range 30.6–35.0 μm), or 10 days of culture (mean range 75.8–95.8 μm). (**G**) Representative images of networks formed at different fibrinogen concentrations, z-projection images were generated from confocal images. Red, F-actin. Scale bar: 300 μm. N = 3; n.s., non significant; *, $p < 0.05$; **, $p < 0.01$; ***, $p < 0.001$.

partment over a 30-min period, using the Lumascope LS720 (Etaluma) live-imaging platform. Using ImageJ (v2.0), vascular permeability was quantified using a parameter termed 'net-fold intensity change/mm^2'. Briefly, the intravascular and extravascular dye intensities were recorded at three regions of interest (ROI) per device (image). Following this, the change in net-fold intensity between intravascular and extravascular zones was characterised at T = 0 and T = 30 min—with a greater fold change indicative of more permeable vessels. T = 0 was determined as when the dye intensity was stable within the vessel, therefore some devices were analysed for shorter time periods (shortest time period being 28 min). The total surface area of the vessel network was then determined using CellProfiler (v4.2.1), by calculating the total tube length and Ferets diameter of the vessel network. Computing the 'net-fold intensity change' and surface area of the vessels allowed us to determine the intravascular-to-extravascular permeability of FITC-dextran, per mm^2.

Nutrient starvation assay. Nutrient starvation is a well-established technique to induce cell-stress, we replicated the assay used by Nashimoto et al.[33]. HUVEC and HUVEC/pericyte microvasculatures were cultured for 7 days. Following this, samples were cultured for a further 3 days in either normal VEGF supplemented EGM-2, or a solution of 90% DPBS and 10% VEGF supplemented EGM-2. Samples were then fixed and stained for CD31/F-actin before imaging.

Toxicity assay. HUVEC and HUVEC/pericyte vasculature networks were cultured for 10 days. To improve openings in the co-culture, 60 × 103 HUVECs were introduced in the later media channel 24 h after seeding in the chips. The chips were then tilted at 90 degrees and incubated for 30 min. The same procedure was repeated in the other media channel. For this assay, two types of particles were used. Silica particles (Bangs Laboratories, average diameter 300 nm) were coated with poly(dimethylaminoethyl methacrylate) (PDMAEMA) following a procedure previously published[34,35]. The final dry diameter of these particles is 330 nm. Titanium oxide (TiO2, anatase- SigmaAldrich) nanoparticles (diameters about 23 nm) are commercially available. Particles were washed with ethanol, centrifuged at 4 k rpm for 10 min and then washed again with water and PBS with cycles of centrifugation in between. Particles were stored in PBS. Before the experiment, particles were sonicated for 5 min and diluted in optiMEM to prevent aggregation due to serum in the medium. The concentrations tested were: 50 and 500 μg/mL for the SiO2 and 100 and 1000 μM for the TiO2[36]. The particles solutions were added in the media wells and cells were incubated for 4 h. Controls were also prepared with optiMEM only. After 4 h, the medium was switched back to VEGF supplemented EGM2. The samples were left for a further 4 days and then fixed and stained for CD31/F-actin.

To confirm particles entered the vasculature, tagged RNA-decorated silica particles were also prepared. Sterile particles were dispersed in PBS and mixed with an equal volume of Cy5 siRNA (Red fluorescent tagged) in RNAse free water, at an N/P ratio of 10. The mixture was then vortexed for 30 s and incubated at RT for 20 min. The mixture was then diluted in optiMEM and added to the media channels of the mature vasculature. After 4 h incubation, the solution was replaced with VEGF supplemented EGM2. Images were acquired using an epifluorescent microscope at several time points in fluorescent and bright field mode.

Immunostaining. Devices were washed with phosphate buffered saline (PBS, Sigma-Aldrich) before fixing in 4% para-formaldehyde (PFA) for 20 min at RT. Samples were then washed with PBS and incubated with 0.4% Triton X-100 solution for 10 min at RT, before washing again with PBS. Next, samples were blocked for 4 h in 3% bovine serum albumin (BSA, Sigma-Aldrich) blocking buffer solution at RT, before overnight incubation (4 °C) with primary antibodies. The following antibodies were used: neural/glial antigen 2 (NG2) monoclonal antibody (9.2.27) Alexa Fluor 488 (eBioscience, 1:100), APC mouse anti-human CD140b (PDGFRβ) (BioLegend, 1:100), Cleaved Caspase-3 (Asp175) monoclonal antibody Alexa Fluor® 555 (Cell Signalling Technology) mouse monoclonal human CD31 Alexa Fluor 488-, 594- and 647-conjugated antibodies (BioLegend; 1:100), mouse monoclonal zona occludens-1 Alexa Fluor 594-conjugated antibody (Thermo Fisher Scientific; 1:200), mouse monoclonal beta-catenin Alexa Fluor 647-conjugated antibody (Thermo Fisher Scientific; 1:100); mouse monoclonal VE-cadherin Alexa Fluor 488-conjugated antibody (Fisher Scientific; 1:100); mouse monoclonal collagen IV (1042) Alexa Fluor 647-conjugated (eBioscience™); mouse monoclonal fibronectin (HFN7.1) Alexa Fluor 647 and 405-conjugated antibody (Novus Biological); rabbit polyclonal laminin antibody (ab11575, abcam). Cell nuclei were stained with DAPI (Sigma-Aldrich; 1:1000) and F-actin filaments were stained using phalloidin (Merck; 1:500 and Thermo Fisher Scientific; 1:40). Samples were then washed with PBS and stored at 4 °C before imaging.

Live/dead assay. In order to assess cytotoxicity after nanoparticle incubation, we used a standard LIVE/DEAD™ Viability/Cytotoxicity Kit from Thermo Fisher at the concentrations recommended by the producer. Chips were washed trice with PBS before incubation with the reagents. Samples were imaged after 30 min incubation.

Image analysis. F-actin or CD31 staining was used to quantify vessel formation and morphology. Following staining, vessels were imaged using the Leica TCS SP2 confocal and multiphoton microscope. 2–3 ROI were selected per chip for imaging and downstream analysis, with each ROI being approximately 1.4 mm^2. Due to the 75 μm height of devices, Z-projections of the microvasculature were captured and merged, before further analysis using CellProfiler (v4.2.1)[37]. To quantify vessel formation, vessel visualisation was first optimised using 'close' and 'clean' functions, followed by skeletonization, which gave a 1-pixel wide skeleton overlay of the vessel network. The total skeleton length was then quantified, termed 'Total Tube Length'. The Feret's diameter of the vessel network was calculated by first quantifying the total pixelated area, prior to skeletonization, then quanti-

fying the total tube length as described above, the total pixelated area was then divided by the total tube length, giving the Feret's diameter.

Fibronectin deposition in the presence or absence of pericytes was measured by quantifying the mean intensity of the protein in the perivascular space. For this, a mask of the network was created using the CD31 staining (images were thresholded and a mask created through the ImageJ function), the areas outside the vasculature were selected and the fibronectin's intensity was measured there.

For cleaved-caspase 3 characterisation and cytotoxicity analysis (via ethidium homodimer-1) after nanoparticle treatment (Sect. "Toxicity assay"), masks of the vascular network were created and the intensity of the marker was measured in the network area only. The intensity was then normalised to that measured in control samples.

Statistical analysis. Statistical analysis was performed on Prism (GraphPad Prism v9.0.0) software. Data was plotted as the mean ± SEM in all graphs. The statistical test conducted depends on the experimental paradigm and includes; unpaired one-tailed student t-test and one-way analysis of variance (ANOVA). Results are shown as mean ± standard error of the mean (SEM). Statistical significance was assumed for $p < 0.05$. * represents $p < 0.05$, ** represents $p < 0.01$, *** represents $p < 0.001$. A minimum of three independent repeats was conducted per experiment, with the total number detailed figure legends. In all figures, summary of statistical analysis is indicated by horizontal bars that start and end at the conditions being compared.

Results and discussion

Development of vascularised microfluidic systems. Microfluidic devices (3 parallel channels separated by micro-pillars, Fig. 1A) were created using photo-lithography, followed by casting of a PDMS replica and bonding to a glass coverslip. This process significantly reduces PDMS hydrophobicity and was found to induce leakage from the central compartment into the side-channels during gel loading. We investigated the recovery of hydrophobic properties of chips and observed partial recovery following storage (72 h), which was enhanced when stored at 60 °C (SI Fig. S1), in agreement with the literature[38,39]. Microfluidic devices which underwent 72 h recovery at 60 °C displayed significant increase in the rate of successful injections, compared with chips which underwent recovery for 72 h at room temperature (100.0 ± 0.0 vs 42.9 ± 20.2%, respectively). All future devices were therefore stored for 72 h at 60 °C following plasma treatment and bonding.

Following the development of our injectable microfluidic devices, we established a basal set of conditions to form a reproducible vasculature. Initial conditions used (SI Table S1) were selected based on protocols found in the literature. We examined the impact of some of these parameters, starting with the density of endothelial cells seeded. In the literature, the endothelial cell density used to form vasculatures in a microfluidic system is in the range of $2 - 20 \times 10^6$ HUVECs/mL[16,24,40]. We selected total tube length and vessel diameters to describe vessel formation following 4-days culture, this time point was initially selected as literature demonstrated this was suitable for the formation of mature vessel networks[16,22]. As shown in Fig. 1B–D, increasing HUVEC densities from 2 to 6×10^6 HUVECs/mL led to a significant increase in total tube length, but had no significant impact on vessel diameter. In addition, no significant difference in total tube length and vessel diameter was observed between 6 and 8×10^6 HUVECs/mL vessel networks, suggesting that 6×10^6 HUVECs/mL is a sufficient cell density to achieve the formation of high density, relatively large vessels within our system.

Fibrinogen is the main hydrogel component in many vascularised microfluidic devices, however, the reported concentration in these studies varies substantially. The impact of this change in fibrinogen concentration is contended, with studies pointing to negative to negligible correlations with vessel formation[19,41]. We investigated the impact of four commonly used fibrinogen concentrations (1.25, 2.5, 7.5 and 10.0 mg/mL) on vasculogenesis at days 4 and 10. HUVECs cultured in 1.25 mg/mL fibrinogen for 4 days almost entirely degraded their surrounding matrix and adhered to the underlying glass substrate (SI Fig. S2A). At higher fibrinogen concentrations however, no significant impact on total tube length or vessel diameter was observed (after either 4 or 10 days of culture, see Fig. 1E–G). However, there does appear to be clear morphological differences between vessels cultured for 4 or 10 days. At day 4, vessels show extensive coverage, characterised by a high total tube length (range between 11.5 and 16.1 mm/field of view) and low vessel diameter (mean range between 29 and 42 μm). By day 10, vessels are characterised by a low total tube length (range between 6.9 and 11.1 mm/field of view) and high vessel diameter (mean range of 65–129 μm). In addition, samples cultured for 10 days are lumenised (SI Fig. S2B-C). This concurrent decrease in total tube length and increase in vessel diameter, between days 4 and 10, suggests vessels are merging to form wider overall tubes, but with a reduced overall network length. This process, reminiscent of hyperplasia, may also be associated with endothelial cell proliferation during prolonged culture times. Investigations of the impact of the presence of collagen 1 within the gel and the concentration of VEGF within the range of 25–150 ng/mL did not indicate any statistically significant difference in total tube formation (but vasculogenesis was severely restricted in the absence of VEGF, SI Figs. S3-4). In addition, aprotinin treatment was only effective at limiting tube formation when supplemented in the media every 24 h. (SI Fig. S5). Overall, the basal conditions we identified to form a reproducible vasculature are detailed in the Supplementary Table S1. Briefly, 6×10^6 HUVECs/mL were cultured in a 10 mg/mL fibrinogen hydrogel for 10 days with the culture medium (EGM-2 containing 50 ng/mL VEGF) replaced every 24 h. Supplementation of fibrinogen gels with collagen or aprotinin was not continued.

Impact of pericytes on vessel structure. Pericytes are an important structural component of the blood vessels and the microvasculature. As such, their incorporation within forming vessel networks in microfluidic devices has been widely studied[15,17,32]. Indeed, co-culturing endothelial cells with pericytes promotes significant morphological changes in the formed vessel networks, including the inhibition of vessel hyperplasia[15].

To limit the apparent hyperplasia observed at day 10 in HUVEC monocultures, we co-cultured endothelial cells and pericytes (10:1, respectively) for 4–10 days, and quantified vessel diameter and total tube length. Similar to what is described in the literature, the introduction of pericytes led to a significant reduction in vessel diameter when compared with endothelial monocultures (36.1 ± 2.5 vs. 52.3 ± 0.9 μm, respectively; culture for 4 days), see Fig. 2. In addition, pericytes had no significant impact on total tube length. When cultured for 10 days, co-cultures maintained a significantly lower vessel diameter, compared with endothelial monocultures (42.5 ± 2.7 vs. 99.6 ± 10.8 μm, respectively). This suggests that pericytes stabilise vessel structure and prevent the occurrence of hyperplasia. In addition, a significant increase in total tube length was observed in co-cultures at day 10, compared to monocultures (13.5 ± 0.6 vs. 9.5 ± 0.5 mm/field of view, respectively, Fig. 2A), in agreement with the literature[17]. To confirm our conclusions, we immunostained co-cultures for the pericyte markers NG2 and PDGFR-β (Fig. 2E). Cells negative for CD31 and positive for these markers can be seen spreading along the basal surface of the microvessels confirming that pericyte populations positive for PDGFR- β and NG2 associate intimately with vascular networks, recapitulating an important aspect of the normal architecture of physiological microvasculatures[29,42].We also confirmed expression of NG2 and PDGFR-β, as well as CD105, via flow cytometry (SI Fig. S6).

To investigate paracrine signalling between pericytes and endothelial cells we developed an alternative chip design incorporating two parallel gel channels (SI Fig. S7). Seeding HUVECs and pericytes in separate parallel compartments, we examined if pericyte paracrine signalling impacted vascular network morphology (no exogenous VEGF was added). Following 4-day culture, the addition of pericytes led to an increase in total tube length (mean ± SEM, 3.2 ± 0.2 vs. 1.4 ± 0.3 mm/field of view), however had no significant impact on vessel diameter. Hence, although some level of paracrine signalling may result in increased stability of vessels and promote tube formation, results were not as marked as in direct co-culture experiments. If culture time was extended in the absence of exogenous VEGF, vessels started to regress following 4-days in all conditions (data not shown).

Impact of pericytes on vessel maturation. In addition to regulating morphological features of the endothelium, pericytes also promote vessel maturity and barrier function[43–45]. To indicate vessel maturation, the expression of several cell–cell junction proteins, notably members of the tight and adherens junctions, are often characterised[15,22,23,46]. We examined the recruitment of tight junction protein ZO-1, and cell adhesion proteins VE-cadherin and β-catenin at cell–cell junctions (see Fig. 3A and SI Fig. S8). Confocal images did not indicate any significant changes in recruitment of these junction markers in co-cultures compared to monocultures. In particular, ZO-1 was clearly recruited at cell–cell junctions, with little diffuse background staining, suggesting that endothelial cells in both conditions form mature endothelial barriers. Similar recruitment patterns were observed for VE-cadherin and β-catenin. Recruitment of these tight and adherens junction proteins is typically considered to indicate vessels which have reached maturation[15,16,22,23,46]. Accordingly, in our system endothelial cells have differentiated into mature vessels following 10-days culture. In addition, endothelial cells typically displayed an elongated phenotype aligned along the length of the vessels. However, in wider vessels some endothelial cells displayed a more cuboidal morphology, with reduced alignment, in particular in endothelial monocultures.

The basement membrane has an important physiological role in the morphology and development of blood vessels and abnormalities have been reported in tumour angiogenesis[47,48]. The presence of pericytes has been shown to regulate the deposition of ECM proteins at the basement membrane[49]. Type IV collagen and laminin are two of the main components of the basement membrane, whereas fibronectin is deposited by fibroblasts and pericytes in the surrounding mesenchymal tissue[50]. We assessed the deposition of these three proteins in mature vasculatures (after 10-days culture) in mono- and co-cultures. Images show that all three proteins were secreted in both conditions and are tightly associated with the vascular network (Fig. 3B and SI Fig. S9). Orthogonal optical sections obtained for collagen IV and laminin indicated proteins deposition at the basement membrane of endothelial networks, in both mono- and co-cultures. However, fibronectin deposition accumulated in interstitial tissue in co-cultures, closely associated with pericytes. Quantification of the perivascular fibronectin deposited adjacent to the vascular network, but not associated with its lamina, confirmed significant levels of fibronectin deposition in the perivascular space in the presence of pericytes, compared to monocultures (Fig. 3B).

Following culture for 10 days, we observed that vessels display both junction marker expression and localisation, and ECM deposition associated with mature microvasculature formation (Fig. 3). Therefore, we next investigated the impact of pericytes on vessel permeability in our system at this time point. Using protocols comparable to those reported by others[15,21,23,33,51], we perfused 70 kDa FITC-dextran through the vessel network. Quantitative analysis of diffusion to interstitial gel areas indicated no change significant difference in the cross-endothelial diffusion of this dye, when comparing HUVEC monocultures and HUVEC/pericyte co-cultures (Fig. 4). Stronger differences in diffusion barrier were reported in the literature, indicative of pericytes contributing to the maturation of the endothelial barrier[17,52]. However, the moderate impact that pericytes had on barrier function is in line with the quality of cell–cell junctions and the basement membrane observed in both mono- and co-cultures.

Therefore, overall, our results indicate that pericytes play a minor role in the development and maintenance of the barrier function of microvascularised networks generated in microfluidic chips. Although significant changes in network morphology are observed in co-cultures, cell–cell junctions appear well established and their impact on barrier function is broadly maintained. However, pericytes had a striking impact on the perivascular matrix remodelling, rather than basement membrane remodelling per se, therefore suggesting that they may play an important role in the stabilisation of vascular networks.

Impact of pericytes on microvasculature stability. Pericytes are important regulators of endothelial survival and vessel integrity[30,31,53]. To investigate this further we compared the impact of nutrient starvation on

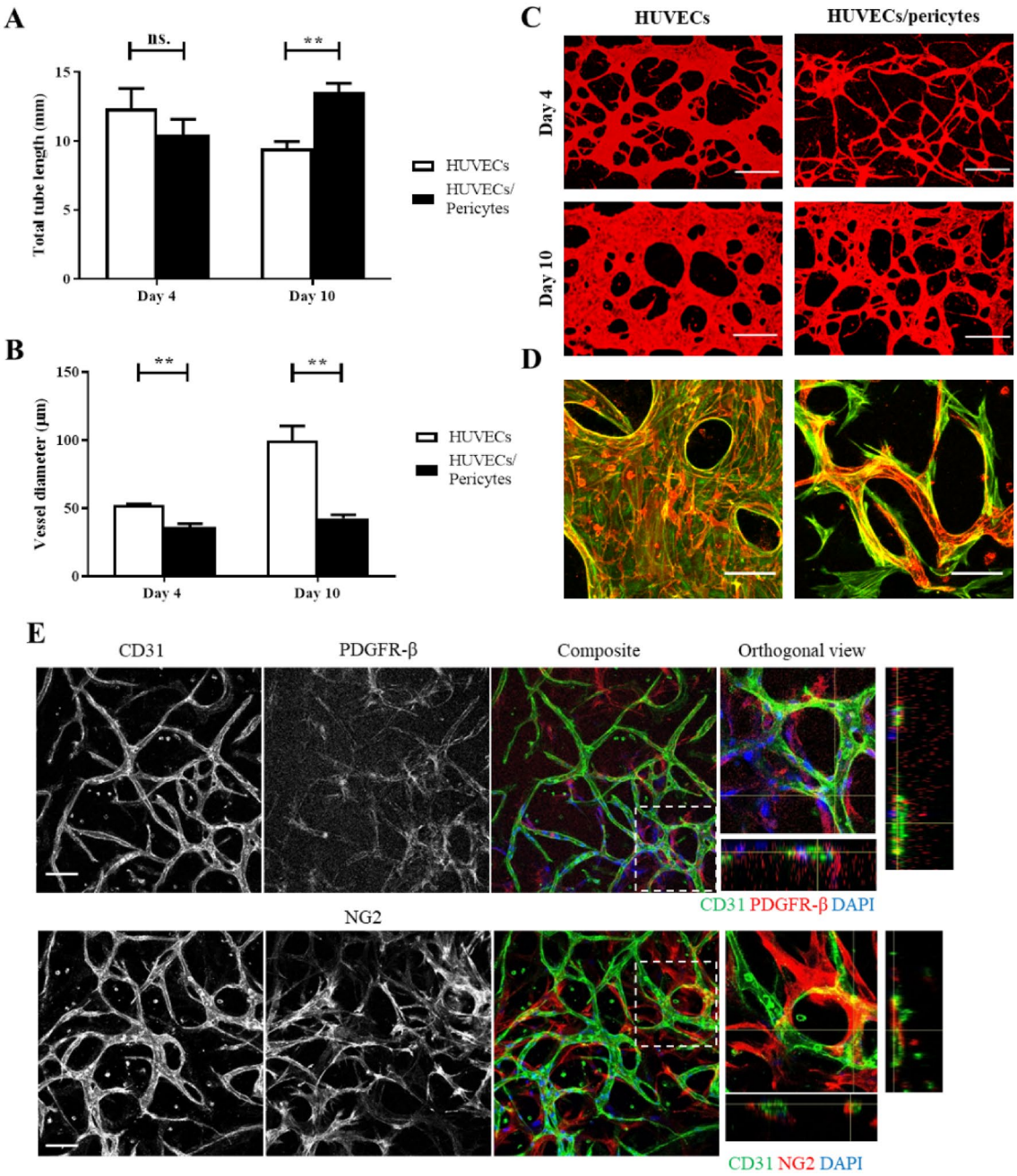

Figure 2. The impact of pericytes on vessel length and diameter. (**A**) In direct co-cultures, pericytes had no significant impact on total tube length at day 4 (mean ± SEM, 12.3 ± 1.5 vs 10.4 ± 1.1 mm/field of view, HUVECs vs HUVEC/pericytes respectively), however, a significant increase in total tube length is seen by day 10 (mean ± SEM, 9.5 ± 0.5 vs 13.5 ± 0.6 mm/field of view, HUVECs vs HUVEC/pericytes respectively). (**B**) The addition of pericytes also led to a significant reduction in vessel diameter following both 4 and 10 days of culture. (**C**) Representative images of samples, z-projection images were generated using confocal images. Red, CD31. Scale bar: 300 µm. (**D**) Representative images showing HUVEC-pericyte interactions, z-projection images were generated using confocal images. Red, CD31. Green, F-actin. Scale bar: 100 µm. N = 3; n.s., non significant; **, $p < 0.01$. (**E**) Cells expressing the pericyte-specific markers PDGFR-β and NG2 (red) are clearly seen at the surface of the microvascular network. Corresponding orthogonal views indicate that these cells are often found wrapping around CD31 positive vessels. Scale bar: 100 µm.

endothelial monocultures and pericyte co-cultures (Fig. 5) using a method adopted from Nashimoto et al.[33]. Serum and nutrient starvation assays are commonly used to investigate environmental stress and apoptosis and have been shown to induce endothelial cell death[54–56]. Following 72 h nutrient deprivation in endothelial monoculture vessel networks, cell–cell adhesion was severely compromised and HUVECs formed small cell aggregates (Fig. 5C), indicative of apoptosis[57]. Interestingly, under identical conditions, co-culture networks retained their

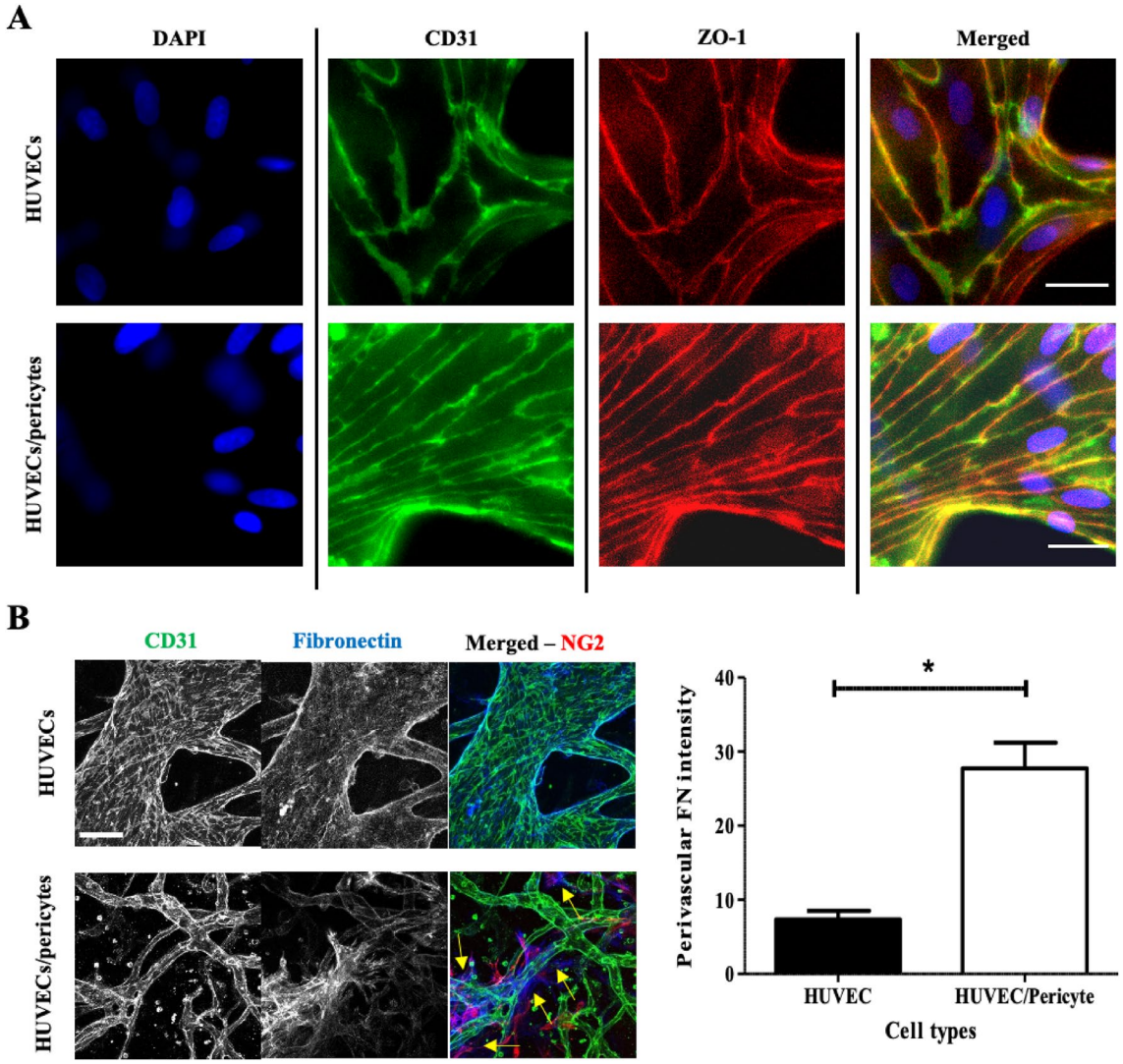

Figure 3. Vessel maturation markers. (**A**) Epifluorescence microscopy images of HUVECs or HUVECs/pericytes vessel networks following 10-day culture, z-projection images were generated using epifluorescence images. These images represent a single Z-frame, displaying junction expression of CD31 and ZO-1. Blue, DAPI. Green, CD31. Red, ZO-1. Scale bar: 25 µm. (**B**) Images displaying fibronectin deposition, z-projection images were generated via confocal microscopy. Blue, Fibronectin. Green, CD31. Red, NG2. Scale bar: 100 µm. Right, quantification of fibronectin deposited in the perivascular space. Yellow arrows indicate some of the perivascular areas in which fibronectin deposition is apparent. N = 3; *, $p < 0.05$.

structure, although a reduction in total tube length was observed, compared to untreated controls (13.5 ± 0.6 vs. 10.7 ± 0.7 mm/field of view, respectively). In addition, nutrient deprivation had no significant impact on co-culture vessel diameter (Fig. 5B). Some single rounded cells were observed in nutrient starved co-cultures, similar to those observed in HUVEC monocultures, although these were much less prevalent. Therefore, our data suggests that pericytes promote the stability and integrity of endothelial networks, even under severe stress conditions. This agrees with observations that pericytes play a role in the survival of endothelial cells[30,31,53].

Considering the impact of pericytes on the stability of networks in response to stress, we proposed that they could play a role in the preservation of network stability in response to toxic compounds such as some nanoparticles. TiO_2 nanoparticles displayed mild toxicity on 2D endothelial layers, disrupting cell–cell junctions and inducing leakiness[36]. We investigated the impact of these nanomaterials (TiO_2 nanoparticles with a diameter of 23 nm), as well as that of other positively charged polymer-coated silica nanoparticles (330 nm diameter with a poly(dimethyl aminoethyl methacrylate) shell). These latter particles are finding applications in gene delivery and are known to induce toxicity in endothelial cells [35]. 100 and 1000 µM TiO_2 nanoparticles displayed a negligible impact on total tube length and vessel diameter in both the mono and co-cultures (SI Fig. S10), in contrast to their impact on endothelial mono-cultures (tube diameters of 137.3 ± 33.1, 106.5 ± 24.4 and 90.2 ± 7.3 µm for the control and 100 and 1000 µM TiO_2 exposed samples, respectively), although this is not significant[36].

In contrast to TiO_2 nanoparticles, cationic PDMAEMA-coated silica nanoparticles displayed a significant effect on the HUVECs microvasculature at both 50 and 500 µg/mL concentrations, destabilising associated

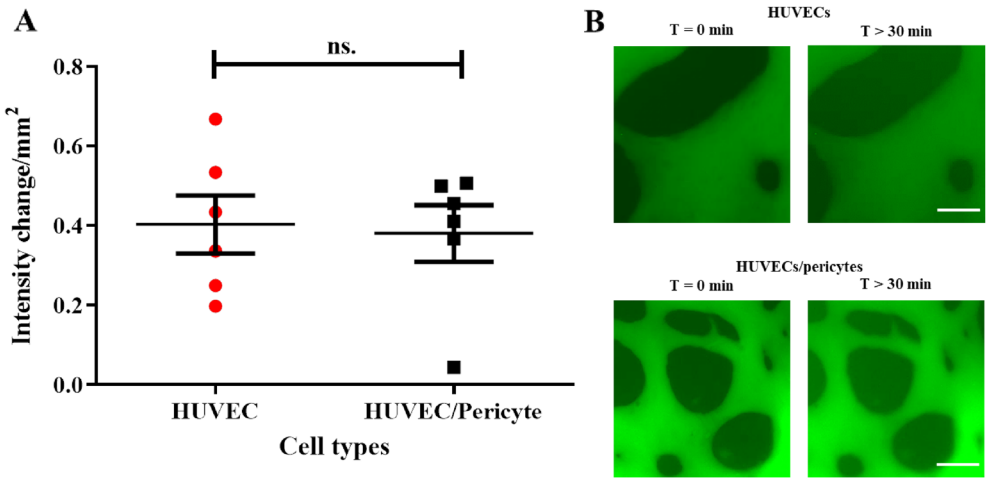

Figure 4. The impact of pericytes on vessel permeability. 70 kDa FITC-dextran was perfused after 10 days of culture. (**A**) Using 'net-fold intensity change/mm^2 to define vessel permeability, the addition of pericytes had no significant impact on endothelial barrier function (mean ± SEM, 0.38 ± 0.07 compared with 0.4 ± 0.07 for endothelial monocultures). (**B**) Representative epifluorescence images at T = 0 and T = 30 min. Scale bar: 100 µm. N = 6; n.s., non significant.

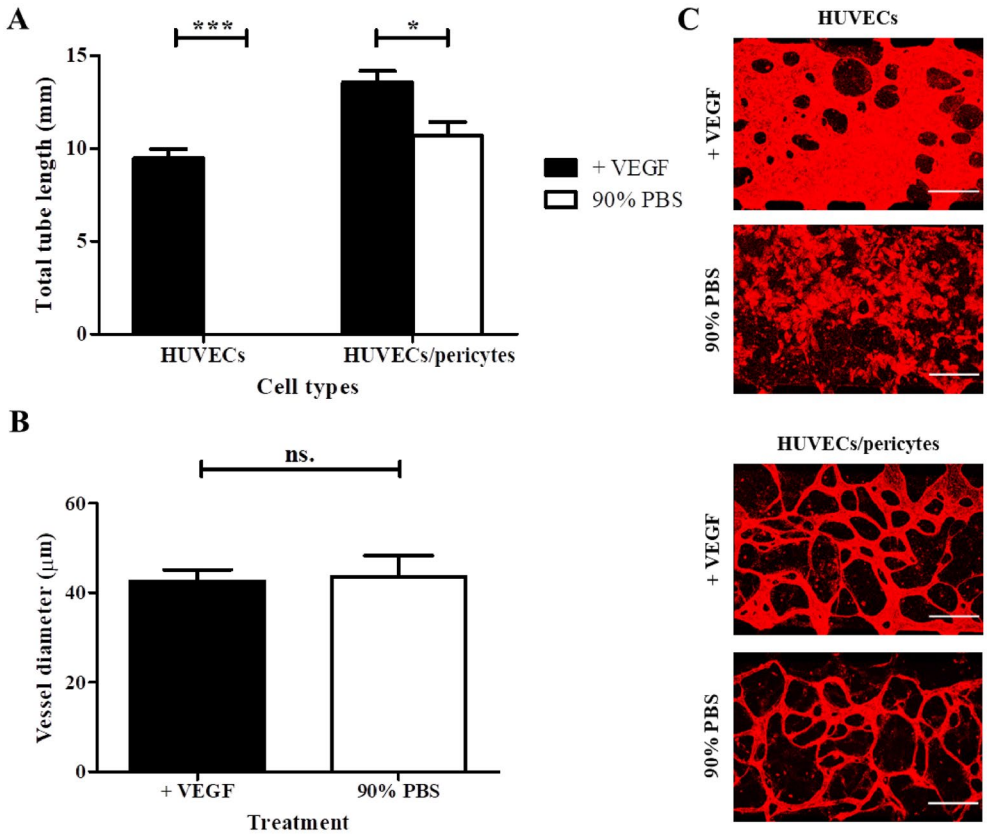

Figure 5. The impact of pericytes on network stability in response to starvation. (**A**) 72 h nutrient starvation resulted in the entire collapse of HUVEC networks in monocultures. In contrast, HUVEC/ pericyte networks persisted, although they apparently regressed compared with untreated conditions (mean ± SEM total tube length, 10.7 ± 0.7 vs 13.5 ± 0.6 mm/field of view, respectively). (**B**) Impact of starvation on tube diameter in co-cultures, showing no significant difference after starvation. (**C**) Representative images, z-projection images were generated using confocal images. Red, CD31. Scale bar: 300 µm. N = 3; n.s., non significant; *, $p < 0.05$; ***, $p < 0.001$.

networks at the highest concentrations tested (Fig. 6A,B). These nanoparticles are based on a silica core, functionalised with dense PDMAEMA brushes. Such cationic polymeric nanomaterials display excellent properties of gene delivery applications, but also some toxicity, as for most polycationic materials[34,58,59]. While the total tube length was not significantly affected, the tube diameter decreased from 137.3 ± 33.1 µm for control to 76.2 ± 13.5 and 49.6 ± 10.6 µm for the 50 and 500 µg/mL, respectively. Associated with these morphological changes, the density of network branches was not significantly affected in co-cultures but clearly increased in the HUVECs networks, reflecting the gradual breakdown of corresponding networks (SI Fig. S11). Overall, images clearly evidenced the disassembly of the networks following exposure to these nanoparticles. However, co-cultured networks remained stable even at the highest concentrations of nanoparticles tested, with no significant impact on total tube length and vessel diameter (Fig. 6, tube diameter is 29.2 ± 2.0 and 24.8 ± 2.3 µm for control and 500 µg/mL particles respectively).

To investigate processes associated with this response to cationic nanoparticles, we assessed apoptosis, through cleaved caspase 3 expression and ethidium homodimer-1 nuclear localisation (Fig. 6C–E and SI Fig. S12). Cleaved caspase 3 expression was significantly higher in nanoparticle-treated monocultures compared

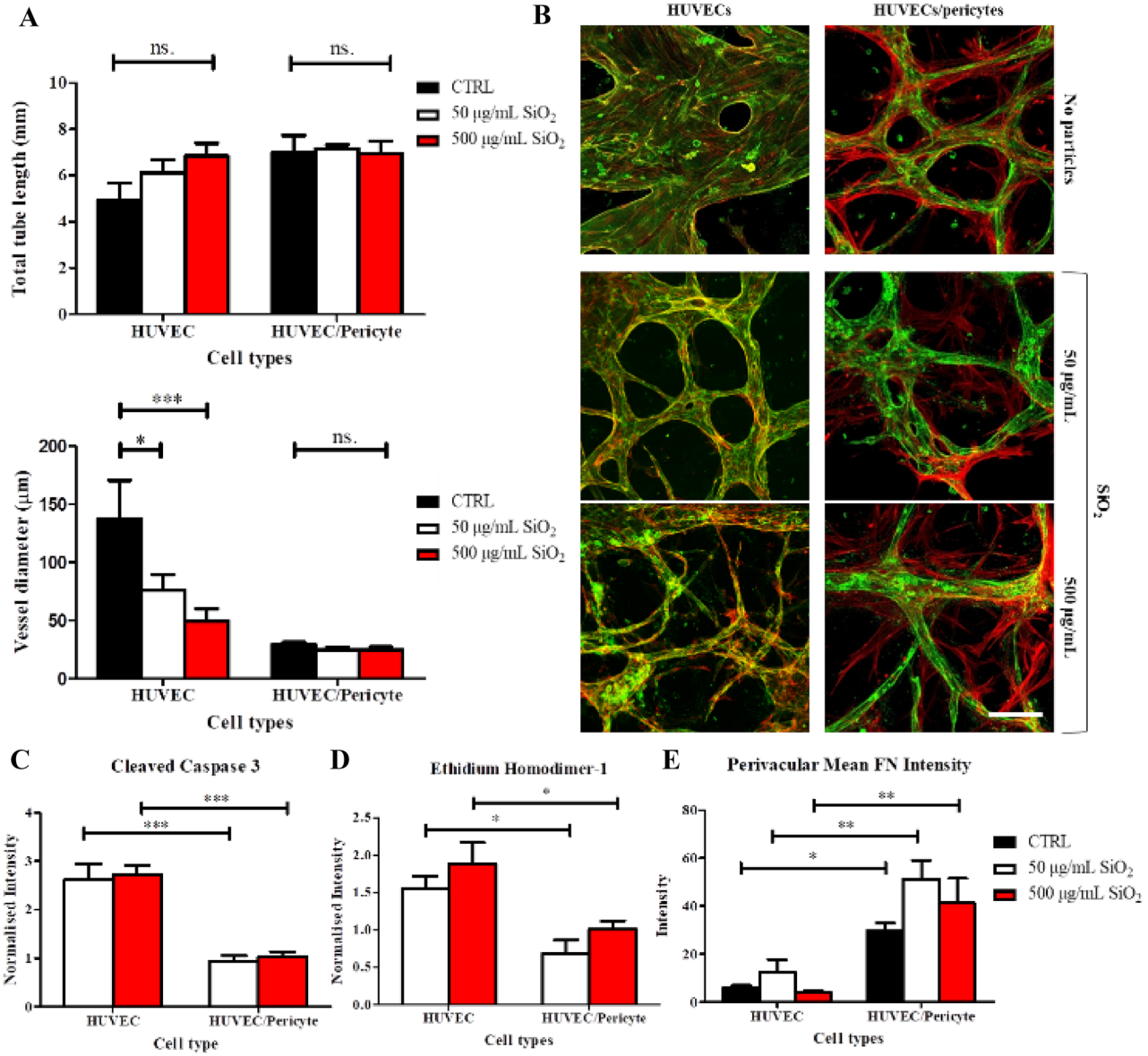

Figure 6. The impact of cationic nanoparticles on vascular network integrity. (**A**) Following 4-day treatment with cationic silica nanoparticles, a significant reduction in vessel diameter is observed in HUVEC monocultures. This is not observed when HUVECs are co-cultured with pericytes. (**B**) Representative images of microvascular networks following treatment with cationic silica nanoparticles, z-projection images were generated using confocal images. Red, F-actin. Green, CD31. Scale bar: 100 µm. (**C–E**) Quantification of relative mean intensity for cleaved caspase 3 (ratio treated/Ctrl) and cytotoxicity via ethidium homodimer-1 (ratio treated/Ctrl) and mean intensity of perivascular fibronectin (FN) deposition. N = 3; n.s., non significant; *, $p < 0.05$; **, $p < 0.01$; ***, $p < 0.001$.

to untreated controls (relative intensity ratios of 2.6 ± 0.3 and 2.7 ± 0.2 at nanoparticle concentrations of 50 and 500 µg/mL, respectively; Fig. 6C). In contrast, cleaved caspase 3 expression in co-culture remained comparable to controls (ratios are 0.9 ± 0.1 and 1 ± 0.09 at nanoparticle concentrations of 50 and 500 µg/mL, respectively). Similarly, ethidium homodimer-1 nuclear localisation increased in monocultures treated with cationic nanoparticles treatment, but not in co-cultures (Fig. 6D). Therefore, our data indicate a protective role of pericytes on nanoparticle-induced apoptosis.

Perivascular fibronectin deposition in response to cationic nanoparticles treatment was next examined (Fig. 6E). Fibronectin deposition was unaltered by nanoparticles exposure in both mono- and co-cultures treated with cationic nanoparticles, compared to untreated controls, but was found to be systematically higher in co-cultures, even after cationic nanoparticles treatment. Hence the increased fibronectin deposition observed in co-cultures was preserved in the context of a nanotoxicity response.

Finally, we confirmed that nanoparticles accumulated in these networks after several hours of treatment, using silica particles loaded with fluorescently labelled RNA (SI Fig. S10). Therefore, our results indicate that, in contrast to the weak impact of the negatively charged TiO_2 nanoparticles, cationic silica nanoparticles resulted in significant cell toxicity, even in a 3D model. However, despite the significant stress induced to the network, pericyte co-culture stabilised associated microvasculatures.

In addition to their anti-apoptotic paracrine effect[30,31], pericytes may contribute to the stability of microvascular networks via other mechanisms. Our results clearly indicate an increased remodelling of the perivascular matrix, with significant fibronectin deposition, which may contribute to the stability of the apico-basal polarity in response to environmental stress, such as in serum starvation and in response to cationic nanoparticles. However, our attempts at stably supressing fibronectin expression in pericytes were unsuccessful (not reported) and did not allow us to investigate such process and establish its significance in pericyte-induced vascular stabilisation. It could also be proposed that other structures associated with vasculature maturity, such as the glycocalyx composition and surface density at the membrane[60], contribute to confer protection from contact toxicity (for example associated with cationic nanoparticles), without significantly regulating barrier function. Further studies are required in order to define the precise mechanism via which pericytes stabilise vascular networks in response to stress and nanotoxicity in vitro and in vivo.

Conclusions

With our model, we quantified the impact of a range of parameters involved in the establishment of a microvasculature in multi-channel microfluidic chips. Our work highlighted the role of pericytes in the stabilisation of vascular networks and the prevention of hyperplasia. We observed that pericytes, through paracrine signalling, promote short-term vessel formation. However, our results indicate that perivascular matrix remodelling contributes to the regulation of vessel hyperplasia and the stabilisation of the vessel plexus. Although we found pericytes had no significant impact on barrier function, pericytes protected the integrity of vascular networks and inhibited vessel regression following nutrient starvation, when compared with endothelial monocultures. Therefore, this work indicates that the main benefit of endothelial cells/pericytes co-culture may be associated with the stabilisation of microvascular networks, long term or in response to challenging media conditions (e.g. in use with alternative media for more complex culture conditions, sometimes serum free). Furthermore, a similar protective response was observed in co-cultures exposed to high concentrations of cationic nanoparticles. These results highlight the importance of pericytes in protecting the microvasculature, and clearly demonstrate that in-vitro models which feature microvasculature stress should incorporate pericytes, to capture their protective effect on endothelial integrity, whether for safety and toxicity testing or to model the progression of diseases. This study also raises new questions relevant to the design of nanotherapeutics. The mechanisms of nanotoxicity to microvasculatures remains to be further explored and the mechanism via which pericytes contribute to the protection of associated microvasculature should be established.

Data availability

The datasets used during the current study are available from the corresponding author on reasonable request.

Received: 6 August 2022; Accepted: 10 March 2023
Published online: 07 April 2023

References

1. Ponce, M. L. Tube formation: An in vitro matrigel angiogenesis assay. *Methods Mol. Biol. Clifton N. J.* **467**, 183–188. https://doi.org/10.1007/978-1-59745-241-0_10 (2009).
2. Huh, D., Matthews, B. D. & Mammoto, A. Reconstituting organ-level lung functions on a chip. *Science* **328**, 1662–1668. https://doi.org/10.1126/science.1188302 (2010).
3. Shin, Y. *et al.* Microfluidic assay for simultaneous culture of multiple cell types on surfaces or within hydrogels. *Nat. Protoc.* **7**, 1247–1259. https://doi.org/10.1038/nprot.2012.051 (2012).
4. Albini, A., Benelli, R., Noonan, D. M. & Brigati, C. The, "chemoinvasion assay": A tool to study tumor and endothelial cell invasion of basement membranes. *Int. J. Dev. Biol.* **48**, 563–571. https://doi.org/10.1387/ijdb.041822aa (2004).
5. Bertulli, C. *et al.* Image-assisted microvessel-on-a-chip platform for studying cancer cell transendothelial migration dynamics. *Sci. Rep.* **8**, 12480–12480. https://doi.org/10.1038/s41598-018-30776-0 (2018).
6. Langhans, S. A. Three-dimensional in vitro cell culture models in drug discovery and drug repositioning. *Front. Pharmacol.* **9**, 6. https://doi.org/10.3389/fphar.2018.00006 (2018).
7. Lee, J., Lilly, G. D., Doty, R. C., Podsiadlo, P. & Kotov, N. A. In vitro toxicity testing of nanoparticles in 3D cell culture. *Small* **5**, 1213–1221. https://doi.org/10.1002/smll.200801788 (2009).
8. Yin, F. *et al.* A 3D human placenta-on-a-chip model to probe nanoparticle exposure at the placental barrier. *Toxicol. In Vitro An Int. J. Publ. Assoc. BIBRA* **54**, 105–113. https://doi.org/10.1016/j.tiv.2018.08.014 (2019).

9. Hassell, B. A. *et al.* Human organ chip models recapitulate orthotopic lung cancer growth, therapeutic responses, and tumor dormancy in vitro. *Cell Rep.* **21**, 508–516. https://doi.org/10.1016/j.celrep.2017.09.043 (2017).
10. Zhang, B., Korolj, A., Lai, B. F. L. & Radisic, M. Advances in organ-on-a-chip engineering. *Nat. Rev. Mater.* **3**, 257–278. https://doi.org/10.1038/s41578-018-0034-7 (2018).
11. Li, Y. *et al.* Atmospheric nanoparticles affect vascular function using a 3D human vascularized organotypic chip. *Nanoscale* **11**, 15537–15549. https://doi.org/10.1039/c9nr03622a (2019).
12. Ahn, J. *et al.* Investigation on vascular cytotoxicity and extravascular transport of cationic polymer nanoparticles using perfusable 3D microvessel model. *Acta Biomater.* **76**, 154–163. https://doi.org/10.1016/j.actbio.2018.05.041 (2018).
13. Oh, S. *et al.* "Open-top" microfluidic device for in vitro three-dimensional capillary beds. *Lab. Chip* **17**, 3405–3414. https://doi.org/10.1039/c7lc00646b (2017).
14. Lee, Y. *et al.* Microfluidics within a well: an injection-molded plastic array 3D culture platform. *Lab. Chip* **18**, 2433–2440. https://doi.org/10.1039/C8LC00336J (2018).
15. Lee, S., Chung, M. & Li Jeon, N. 3D brain angiogenesis model to reconstitute maturation of functional human blood-brain barrier in vitro. *BioRxiv* https://doi.org/10.1101/471334 (2018).
16. Kim, S., Lee, H., Chung, M. & Jeon, N. Engineering of functional, perfusable 3D microvascular networks on a chip. *Lab. Chip* **13**, 1489–1500. https://doi.org/10.1039/C3LC41320A (2013).
17. Kim, J. *et al.* Engineering of a biomimetic pericyte-covered 3D microvascular network. *PLoS ONE* **10**, 133880. https://doi.org/10.1371/journal.pone.0133880 (2015).
18. Zervantonakis, I. K. *et al.* Three-dimensional microfluidic model for tumor cell intravasation and endothelial barrier function. *Proc. Natl. Acad. Sci.* **109**, 13515–13520. https://doi.org/10.1073/pnas.1210182109 (2012).
19. Whisler, J. A., Chen, M. B. & Kamm, R. D. Control of perfusable microvascular network morphology using a multiculture microfluidic system. *Tissue Eng. Part C Methods* **20**, 543–552. https://doi.org/10.1089/ten.TEC.2013.0370 (2014).
20. Kyoko, Y. *et al.* Construction of continuous capillary networks stabilized by pericyte-like perivascular cells. *Tissue Eng. Part A* **25**, 499–510. https://doi.org/10.1089/ten.tea.2018.0186 (2019).
21. Sobrino, A. *et al.* 3D microtumors in vitro supported by perfused vascular networks. *Sci. Rep.* **6**, 31589. https://doi.org/10.1038/srep31589 (2016).
22. Jeon, J. S. *et al.* Human 3D vascularized organotypic microfluidic assays to study breast cancer cell extravasation. *Proc. Natl. Acad. Sci.* **112**, 214–219. https://doi.org/10.1073/pnas.1417115112 (2015).
23. Jeon, J. S. *et al.* Generation of 3D functional microvascular networks with human mesenchymal stem cells in microfluidic systems. *Integr. Biol.* **6**, 555–563. https://doi.org/10.1039/C3IB40267C (2014).
24. Nagaraju, S., Truong, D., Mouneimne, G. & Nikkhah, M. Microfluidic tumor-vascular model to study breast cancer cell invasion and intravasation. *Adv. Healthc. Mater.* **7**, 1701257. https://doi.org/10.1002/adhm.201701257 (2018).
25. Sims, D. E. The pericyte–a review. *Tissue Cell* **18**, 153–174. https://doi.org/10.1016/0040-8166(86)90026-1 (1986).
26. Dias Moura Prazeres, P. H. *et al.* Pericytes are heterogeneous in their origin within the same tissue. *Develop. Biol.* **427**, 6–11. https://doi.org/10.1016/j.ydbio.2017.05.001 (2017).
27. Yamazaki, T. & Mukouyama, Y. S. Tissue specific origin, development, and pathological perspectives of pericytes. *Front. Cardiovasc. Med.* **5**, 78. https://doi.org/10.3389/fcvm.2018.00078 (2018).
28. Smyth, L. C. D. *et al.* Markers for human brain pericytes and smooth muscle cells. *J. Chem. Neuroanat.* **92**, 48–60. https://doi.org/10.1016/j.jchemneu.2018.06.001 (2018).
29. Armulik, A., Genove, G. & Betsholtz, C. Pericytes: Developmental, physiological, and pathological perspectives, problems, and promises. *Dev. Cell* **21**, 193–215. https://doi.org/10.1016/j.devcel.2011.07.001 (2011).
30. Darland, D. C. *et al.* Pericyte production of cell-associated VEGF is differentiation-dependent and is associated with endothelial survival. *Dev. Biol.* **264**, 275–288 (2003).
31. Franco, M., Roswall, P., Cortez, E., Hanahan, D. & Pietras, K. Pericytes promote endothelial cell survival through induction of autocrine VEGF-A signaling and Bcl-w expression. *Blood* **118**, 2906–2917. https://doi.org/10.1182/blood-2011-01-331694 (2011).
32. Yamamoto, K. *et al.* The stabilization effect of mesenchymal stem cells on the formation of microvascular networks in a microfluidic device. *J. Biomech. Sci. Eng.* **8**, 114–128. https://doi.org/10.1299/jbse.8.114 (2013).
33. Nashimoto, Y. *et al.* Integrating perfusable vascular networks with a three-dimensional tissue in a microfluidic device. *Integr. Biol.* **9**, 506–518. https://doi.org/10.1039/c7ib00024c (2017).
34. Li, D., Sharili, A. S., Connelly, J. & Gautrot, J. E. Highly stable RNA capture by dense cationic polymer brushes for the design of cytocompatible, serum-stable siRNA delivery vectors. *Biomacromol* **19**, 606–615 (2018).
35. Li, D. *et al.* Core-independent approach for polymer brush-functionalised nanomaterials with a fluorescent tag for RNA delivery. *Chem. Commun.* **55**, 14166–14169. https://doi.org/10.1039/C9CC05790K (2019).
36. Setyawati, M. I. *et al.* Titanium dioxide nanomaterials cause endothelial cell leakiness by disrupting the homophilic interaction of VE–cadherin. *Nat. Commun.* **4**, 1673. https://doi.org/10.1038/ncomms2655 (2013).
37. Jones, T. R. *et al.* Cell profiler analyst: Data exploration and analysis software for complex image-based screens. *BMC Bioinform.* **9**, 482. https://doi.org/10.1186/1471-2105-9-482 (2008).
38. Eddington, D. T., Puccinelli, J. P. & Beebe, D. J. Thermal aging and reduced hydrophobic recovery of polydimethylsiloxane. *Sens. Actuators, B Chem.* **114**, 170–172. https://doi.org/10.1016/j.snb.2005.04.037 (2006).
39. Owen, M. J. & Smith, P. J. Plasma treatment of polydimethylsiloxane. *J. Adhes. Sci. Technol.* **8**, 1063–1075. https://doi.org/10.1163/156856194X00942 (1994).
40. Chen, M. B., Whisler, J. A., Jeon, J. S. & Kamm, R. D. Mechanisms of tumor cell extravasation in an in vitro microvascular network platform. *Integr. Biol.* **5**, 1262–1271. https://doi.org/10.1039/c3ib40149a (2013).
41. Ghajar, C. M. *et al.* The effect of matrix density on the regulation of 3-D capillary morphogenesis. *Biophys. J.* **94**, 1930–1941. https://doi.org/10.1529/biophysj.107.120774 (2008).
42. Birbrair, A. *et al.* Pericytes at the intersection between tissue regeneration and pathology. *Clin. Sci. (Lond)* **128**, 81–93. https://doi.org/10.1042/CS20140278 (2015).
43. Luissint, A.-C., Artus, C., Glacial, F., Ganeshamoorthy, K. & Couraud, P.-O. Tight junctions at the blood brain barrier: Physiological architecture and disease-associated dysregulation. *Fluids Barriers CNS* **9**, 23–23. https://doi.org/10.1186/2045-8118-9-23 (2012).
44. Daneman, R., Zhou, L., Kebede, A. A. & Barres, B. A. Pericytes are required for blood-brain barrier integrity during embryogenesis. *Nature* **468**, 562–566. https://doi.org/10.1038/nature09513 (2010).
45. Alcendor, D. J. Human Vascular Pericytes and Cytomegalovirus Pathobiology. *Int. J. Mol. Sci.* **20**, 1456. https://doi.org/10.3390/ijms20061456 (2019).
46. Yeon, J. H., Ryu, H. R., Chung, M., Hu, Q. P. & Jeon, N. L. In vitro formation and characterization of a perfusable three-dimensional tubular capillary network in microfluidic devices. *Lab. Chip.* **12**, 2815–2822. https://doi.org/10.1039/c2lc40131b (2012).
47. Kubota, Y., Kleinman, H. K., Martin, G. R. & Lawley, T. J. Role of laminin and basement membrane in the morphological differentiation of human endothelial cells into capillary-like structures. *J. Cell Biol.* **107**, 1589–1598. https://doi.org/10.1083/jcb.107.4.1589 (1988).
48. Baluk, P., Morikawa, S., Haskell, A., Mancuso, M. & McDonald, D. M. Abnormalities of basement membrane on blood vessels and endothelial sprouts in tumors. *Am. J. Pathol.* **163**, 1801–1815. https://doi.org/10.1016/S0002-9440(10)63540-7 (2003).

49. Stratman, A. N., Malotte, K. M., Mahan, R. D., Davis, M. J. & Davis, G. E. Pericyte recruitment during vasculogenic tube assembly stimulates endothelial basement membrane matrix formation. *Blood* **114**, 5091–5101. https://doi.org/10.1182/blood-2009-05-222364 (2009).
50. Jayadev, R. & Sherwood, D. R. Basement membranes. *Curr. Biol.* **27**, R207–R211. https://doi.org/10.1016/j.cub.2017.02.006 (2017).
51. Moya, M. L., Hsu, Y.-H.H., Lee, A. P., Hughes, C. C. & George, S. C. In vitro perfused human capillary networks. *Tissue Eng. Part C, Methods* **19**, 730–737. https://doi.org/10.1089/ten.tec.2012.0430 (2013).
52. Nakagawa, S. *et al.* A new blood–brain barrier model using primary rat brain endothelial cells, pericytes and astrocytes. *Neurochem. Int.* **54**, 253–263. https://doi.org/10.1016/j.neuint.2008.12.002 (2009).
53. Papapetropoulos, A. *et al.* Direct actions of angiopoietin-1 on human endothelium: evidence for network stabilization, cell survival, and interaction with other angiogenic growth factors. *Lab. Invest.* **79**, 213–223 (1999).
54. Rashid, M.-U. & Coombs, K. M. Serum-reduced media impacts on cell viability and protein expression in human lung epithelial cells. *J. Cell. Physiol.* **234**, 7718–7724. https://doi.org/10.1002/jcp.27890 (2019).
55. Domigan, C. K. *et al.* Autocrine VEGF maintains endothelial survival through regulation of metabolism and autophagy. *J. Cell Sci.* **128**, 2236–2248. https://doi.org/10.1242/jcs.163774 (2015).
56. Yang, Z. *et al.* Autophagy protects the blood-brain barrier through regulating the dynamic of claudin-5 in short-term starvation. *Front. Physiol.* **10**, 2–2. https://doi.org/10.3389/fphys.2019.00002 (2019).
57. Elmore, S. Apoptosis: A review of programmed cell death. *Toxicol. Pathol.* **35**, 495–516. https://doi.org/10.1080/01926230701320337 (2007).
58. Qu, F., Li, D., Ma, X., Chen, F. & Gautrot, J. E. A kinetic model of oligonucleotide-brush interactions for the rational design of gene delivery vectors. *Biomacromol* **20**, 2218–2229 (2019).
59. Raynold, A. A., Li, D., Chang, L. & Gautrot, J. Competitive binding and molecular crowding regulate the cytoplasmic interactome of non-viral polymeric gene delivery vectors. *Nat. Commun.* **12**, 6445 (2021).
60. Weinbaum, S., Tarbell, J. M. & Damiano, E. R. The structure and function of the endothelial glycocalyx layer. *Annu. Rev. Biomed. Eng.* **9**, 121–167 (2007).

Acknowledgements

Funding from the National Centre for the Replacement, Refinement and Reduction of Animals in Research (NC3Rs, NC/M001636/1 and NC/T2T0319), Cancer Research UK (Programme Grants C587/A16354 and C587/A25714) and from the European Research Council (ProLiCell, 772,462 and CANBUILD, 32,566) is gratefully acknowledged.

Author contributions

M.D. and S.D.C. developed the methodologies. F.B. and J.E.G. developed the concept. M.D. and S.D.C. carried out experiments and analysed the data gathered. F.B. and J.E.G. supervised the project and obtained funding for this research. M.D., S.D.C., F.B. and J.E.G. wrote the manuscript and reviewed it.

Competing interests

The authors declare no competing interests.

Additional information

Supplementary Information The online version contains supplementary material available at https://doi.org/10.1038/s41598-023-31352-x.

Correspondence and requests for materials should be addressed to J.E.G.

Reprints and permissions information is available at www.nature.com/reprints.

Publisher's note Springer Nature remains neutral with regard to jurisdictional claims in published maps and institutional affiliations.